J Wood Sci (2011) 57:395–400
DOI 10.1007/s10086-011-1195-9

ORIGINAL ARTICLE

Nobuo Sobue · Kentarou Doi · Munehiro Date

New impedance measurement system estimating cross-sectional moisture distribution in cylindrical bodies and electric network modeling

Received: December 28, 2010 / Accepted: April 13, 2011 / Published online: July 16, 2011

Abstract This work aimed to measure the cross-sectional moisture distribution in a cylindrical body using a double-glass-tube model filled with water and to construct an electric network model that explains the effects of moisture distribution. A new impedance measurement system introducing an intermediate electrode was exploited. The electrode was used to segregate the target local current from the whole current in a cross section of a specimen. Three model cylinders with different moisture distributions were used, and absolute values of impedance and phase were measured over the frequency range 1 kHz to 1 MHz. By introducing an intermediate electrode, frequency responses of the impedance and the phase showed characteristic changes in the high-frequency range associated with the moisture distributions. The trends were simulated numerically by using electric network analysis. The proposed method enabled measurement of a selective current path in the cross section of a cylindrical body.

Key words Impedance measurement · High frequency · Intermediate electrode · Moisture distribution · Electrical model

Introduction

Moisture measurement in logs and standing trees is a key technology not only for improvement of timber drying but also for nondestructive evaluation, especially for segregating logs and standing trees with high moisture content. At present, X-ray computed tomography (CT),[1] magnetic resonance imaging (MRI),[2] and neutron beam imaging[3] methods are efficient as nondestructive tests of the cross-sectional moisture distribution of logs and standing trees, but these techniques are too expensive for everyday use in wood industries. A lateral vibration technique for estimating the core moisture content of standing trees has been also proposed,[4] but the method shows wide deviation of estimated moisture content. Electrical techniques are currently used for portable moisture meters, and some electric meters of the dielectric type are approved as practical tools for sawn softwood timbers.[5] This equipment makes relatively deep penetration of the electric field into timber possible, but they are not able to detect the moisture content in the core parts of logs and standing trees. Some impedance techniques have been studied for timber[6–10] and logs[11] from the point of view of tomography methods, but they have not been adequately developed for application to logs and standing trees.

Our impedance method introduces an intermediate electrode between the supply and detection electrodes and could segregate a target electric current, enabling enhanced measurement of impedance in the cross section of a cylindrical body.[12] In preliminary measurements applied to wood branches during natural drying, we found a particular change in the impedance frequency response curves that showed a peak or a local increase in the high-frequency range;[13] this change was caused by the moisture gradient in the specimen. The present work was conducted to analyze the effect of the cross-sectional moisture distribution on impedance measurement by using glass tube models and to form an electrical network model explaining the cross-sectional moisture distribution of cylindrical bodies.

N. Sobue (✉) · K. Doi
Faculty of Agriculture, Shizuoka University, 836 Ohya, Suruga-ku, Shizuoka 422-8529, Japan
Tel. +81-54-238-4855; Fax +81-54-237-3028
e-mail: afnsobu@ipc.shizuoka.ac.jp

M. Date
Kobayasi Institute of Physical Research, Kokubunji, Tokyo 185-0022, Japan

Part of this article was presented at the 59th (Matsumoto, March 2009) and the 60th (Miyazaki, March 2010) Annual Meetings of the Japan Wood Research Society

Materials and methods

Basic concept of the new impedance measurement

Figure 1 shows a schematic explaining the effect of the intermediate electrode for the proposed impedance mea-

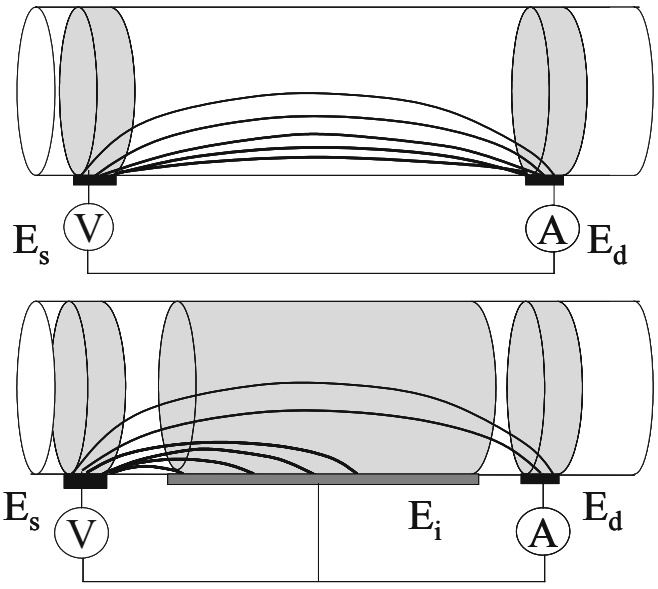

Fig. 1. Schematic of the effect of the intermediate electrode. *V*, supplied voltage; *A*, ampere meter; E_s, supply electrode; E_d, detection electrode; E_i, intermediate electrode

surement. Without the intermediate electrode, all electric field lines which start from the supply electrode end at the detection electrode, which is connected to an impedance meter. On the other hand, the intermediate electrode traps some of the electric field lines and they are introduced into a voltage source. Accordingly, the remained electric field lines, which are located in the core part of the cylindrical body, are collected and introduced into the impedance meter. This means that the impedance of the core part can be selectively measured by introducing the intermediate electrode. The trapping of the electric field lines by the intermediate electrode induces a change in the frequency response of the impedance.

Basic concept of the electric network for double-cylinder models

Three different cylinder models composed of two glass tubes with different diameters are considered, as shown in Fig. 2. The outer space, inner space, or both are filled with water. The outer space represents sapwood and the inner space represents heartwood in the cross section of a log.

The effect of moisture distributions on the impedance frequency response was analyzed by using network analysis of equivalent electric circuits.[14] The network model shown in Fig. 3 was composed of two kind of elements, i.e., resistors and capacitors, and was made up of three groups: (1) capacitors (C_E and C_{Ei}) between the electrodes on the surface of outer tube and the water inside the tube, (2) resistors and capacitors for water in the tube (*R* and *C*) between the supply and the detection electrode or the intermediate electrode, and (3) the capacitor and the resistor for water in the tube (C_p and R_p) between the supply and detection electrodes. As an approximation, resistors connected in parallel

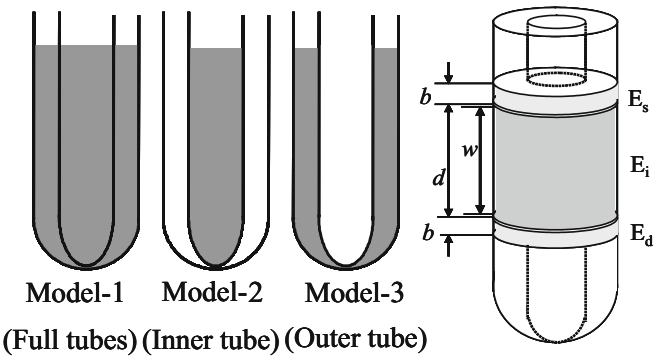

Fig. 2. Cylinder models. *b*, width of supply and detection electrodes; *d*, electrode distance; *w*, intermediate electrode width

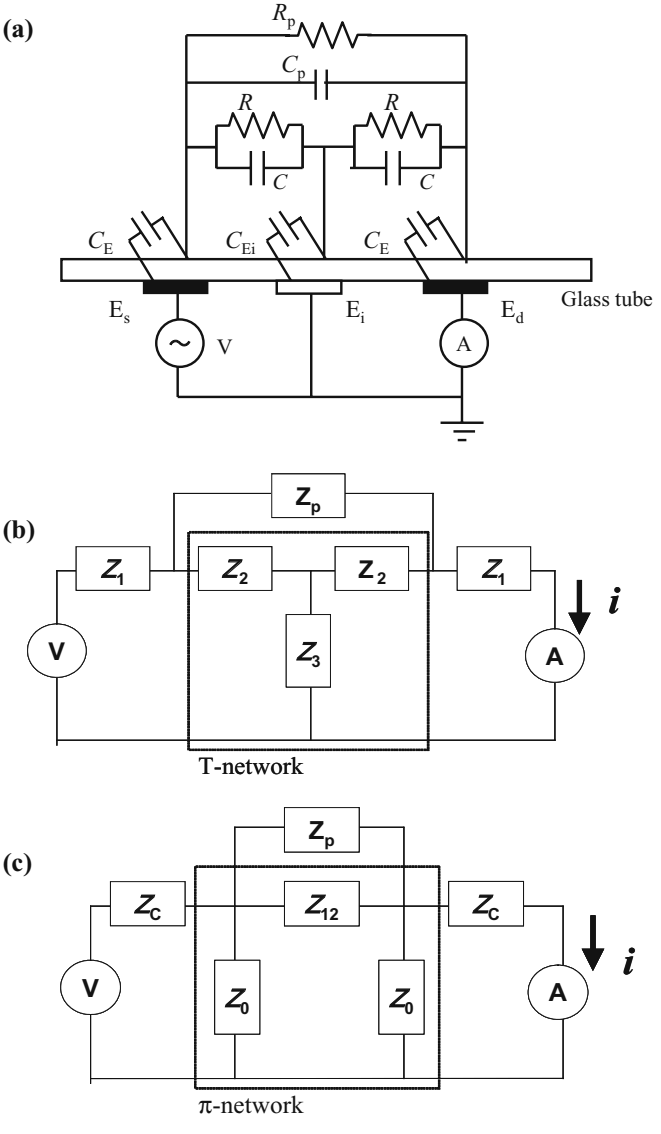

Fig. 3. Equivalent electric network of the cylinder model. **a** Base network, **b** simplified representation by the equivalent T-network, and **c** simplified representation by the equivalent π-network. *R*, resistances; *C*, capacitances; *Z*, impedance elements; *i*, current

with capacitors C_E and C_{Ei} are ignored because the glass tube is an insulator. The target impedance Z is then defined as the ratio of the excitation voltage V to current i in the network model. The impedance meter gives absolute values of the impedance $|Z|$ and the phase θ, i.e., the phase is defined as the phase difference between the detected current and the applied voltage:

$$Z = \Re(Z) + j\Im(Z) \tag{1}$$

$$\theta = \tan^{-1}\frac{\Im(Z)}{\Re(Z)} \tag{2}$$

The original network model was partially rewritten for convenience of mathematical treatment. The T-network in Fig. 3b was transformed into an electrically equivalent π-network in Fig. 3c.[15] The impedance parameters in Fig. 3 are given as follows.

$$Z_1 = Z_C = \frac{1}{j\omega C_E},\ Z_2 = \frac{R}{1+j\omega CR},\ Z_3 = \frac{1}{j\omega C_{Ei}},\quad Z_p = \frac{R_p}{1+j\omega C_p R_p} \tag{3}$$

$$Z_0 = Z_2 + 2Z_3,\ Z_{12} = 2Z_2 + \frac{Z_2^2}{Z_3} \tag{4}$$

$$\frac{1}{Z_T} = \frac{1}{Z_p} + \frac{1}{Z_{12}} \tag{5}$$

Finally, the target impedance Z is given by,

$$Z = \frac{V}{i} = Z_C\left\{\frac{Z_T}{Z_0}\left(\frac{Z_C}{Z_0}+1\right)+\frac{Z_C}{Z_0}\right\}+(Z_C+Z_T)\left(\frac{Z_C}{Z_0}+1\right)+Z_C \tag{6}$$

Experimental setup of cylinder models

The cylinder models were composed of two glass tubes with different diameters as shown in Fig. 2. The outer tube diameter was 30 mm and the inner tube diameter was 19 mm. The outer space, inner space, or both spaces were filled with distilled water.

Ring shaped aluminum electrodes were attached around the outside of the outer tube. The widths of the supply (E_s) and detection (E_d) electrodes were 20 mm. We call the shortest distance between the supply and detection electrodes, d, the electrode distance. We located the intermediate electrode (E_i) between the supply and detection electrodes; the nominal width of the intermediate electrode was varied between 20 and 80 mm. There net width, w, is shorter than the electrode distance by 2 mm because of the clearances of 1 mm between the supply or detection electrode and the intermediate electrode.

An impedance meter (HIOKI LCR 3531 Z) was used to measure the absolute value and the phase of the impedance over the frequency range 1 kHz to 1 MHz. Open and short circuit compensation was done before measurement to cancel the effect of cable impedance between the impedance meter and the electrodes. The measurement was done at room temperature, i.e., about 20°C.

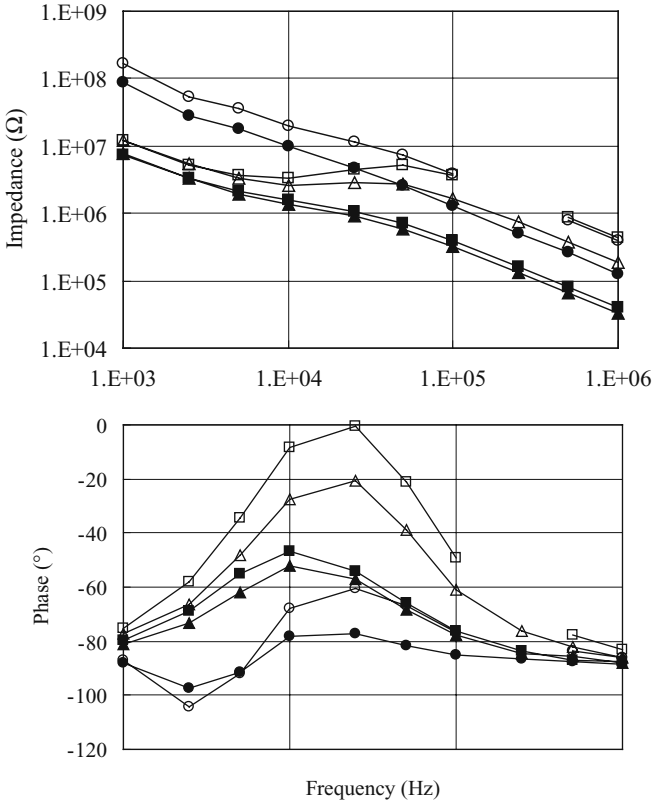

Fig. 4. Frequency characteristics of the impedance and the phase. *Solid symbols*, without the intermediate electrode; *open symbols*, with the intermediate electrode; *triangles*, water in all spaces; *squares*, water in the outer tube; *circles*, water in the inner tube; supply and detection electrodes widths, 20 mm; intermediate electrode width, 40 mm

Results and discussion

Effect of water distribution and the intermediate electrode on impedance and phase

Figure 4 shows the frequency responses of the impedance and the phase for three different water distributions. The water distributions in the glass tubes very much affected these responses. In the case without the intermediate electrode (solid symbols), the logarithm of the impedance decreased almost linearly with the increase of the logarithm of the frequency. On the other hand, by introducing the intermediate electrode (open symbols), a marked local increase (or shoulder) of impedance was apparent in the high-frequency range. The phase shows a large increase as a result of introduction of the intermediate electrode. A phase peak appears in association with the large impedance change. The largest changes occurred when the water was present only in the outer glass tube. This situation may occur when a standing tree has core decay. An intermediate change occurred when all spaces were filled with water. This situation may occur in general cases of logs and standing trees under green conditions. The least change occurred when the water was present only in the inner glass tube. This situation may occur when drying has been carried out for some time and a steep moisture gradient occurs in a log. The

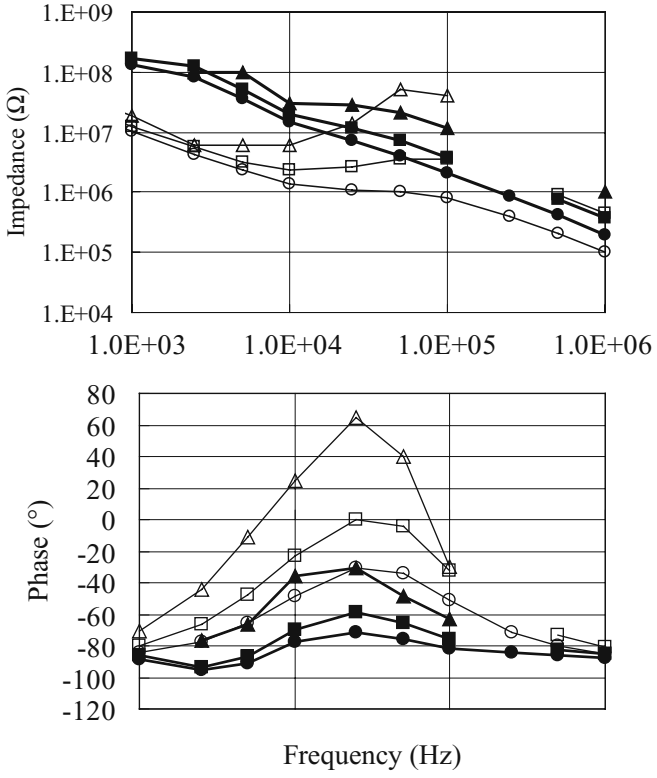

Fig. 5. Effect of the intermediate electrode width on the impedance and the phase. *Open symbols*, water in the outer tube only; *solid symbols*, water in the inner tube only. The widths of the intermediate electrode were 20, 40, and 80 mm, *circles*, *squares*, and *triangles*, respectively

increases of the impedance and the phase in the high-frequency range were very particular, and these specific responses were found in our preliminary measurement during a drying process of sugi branches.[13] The phenomenon looks like the effect of a local resonance associated with an inductor, and we explain the cause by using the electric network model in the following section. As shown in Fig. 4, the introduction of the intermediate electrode enhances the effect of the water distribution.

Figure 5 shows the effect of the width of the intermediate electrode on the impedance for two extreme moisture distributions: model 2 (water in the inner tube only, solid symbols) and model 3 (water in the outer tube only, open symbols). The width of the intermediate electrode affects the impedances considerably in the high-frequency range. The magnitude of the impedance depended on the spatial water distributions. When the outer tube was filled with water (open symbols), for an 80-mm intermediate electrode, the impedance showed a dramatic increase above 10 kHz and the phase increased beyond 0°.

Simulation of the frequency responses of the impedance and the phase

Individual electric constants of the elements were obtained by a trial-and-error method in order to fit the impedance and phase curves for the two extreme models, model 2 and model 3, as shown in Table 1. Prior to the curve fitting, the effect of the electric constant for each element on the target impedance curve was simulated and the major constants that affected the basic form of the impedance curve were chosen; then minor constants were chosen to obtain a better fit. The lines indicating the impedance and the phase in Fig. 6 were generated using the individual electric constants found by curve fitting as described above. Figure 6 shows that the simulation results quantitatively well represent the frequency responses of the impedance and the phase that are shown in Fig. 4. The local increase, or shoulder, of the impedance change is marked when water is present in the outer tube only, and the magnitude of the impedance is larger at low frequencies when the inner tube only is filled with water. The particular impedance and phase changes were thus well simulated by a network model composed of resistors and capacitors only. The electric constants shown

Table 1. Electric constants used for investigating the effect of water distribution were obtained from trial and error fitting to the impedance and phase curves

Model	R (MΩ)	C (pF)	R_p (MΩ)	C_p (pF)	C_E (pF)	C_{Ei} (pF)
Model 2	7	3	5	0.4	3.5	10
Model 3	0.5	0.8	4	0.3	50	100

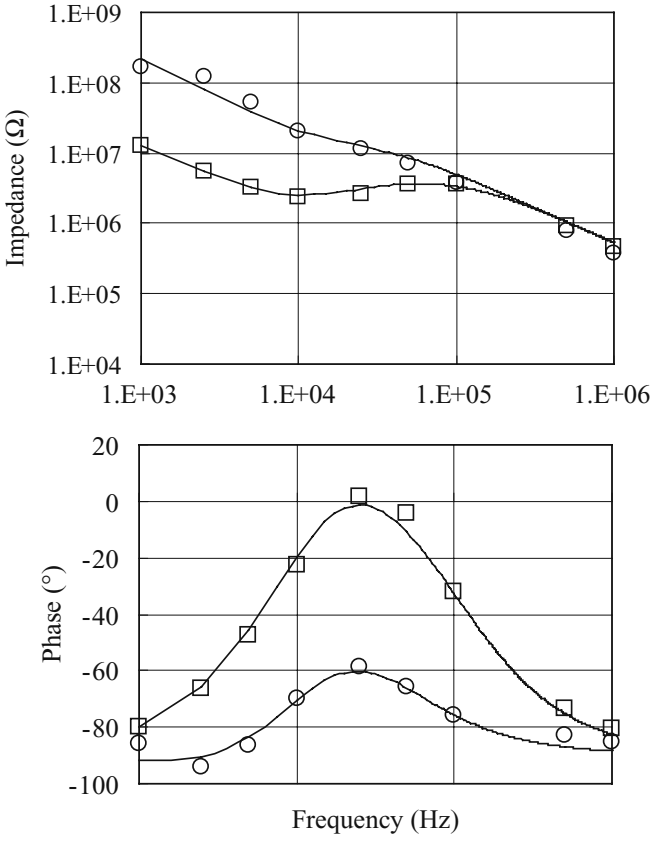

Fig. 6. Simulation results of the frequency characteristics of the impedance and the phase. *Symbols*, experiment; *lines*, calculation; *squares*, water in the outer tube only; *circles*, water in the inner tube only

Table 2. Electric constants for inspecting the local parallel resonance

Model	R (MΩ)	C (pF)	R_p (MΩ)	C_p (pF)	C_E (pF)	C_{Ei} (pF)
Model 3	0.5	0.8	4	0.3	50	100

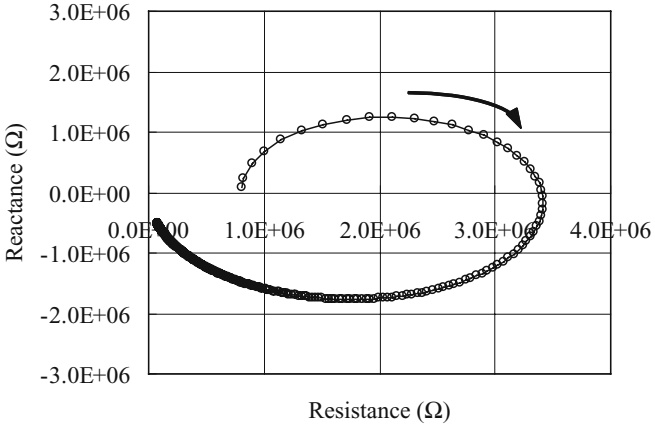

Fig. 7. Impedance plane figure of the local parallel resonance composed of elements Z_{12} and Z_p

in Table 1 reflect the spatial configuration of the moisture distributions. The capacitance C and the resistance R were much larger and the resistance R_p and the capacitance C_p were a little larger when the inner tube alone was filled with water. The capacitances C_E and C_{Ei} were smaller when the inner tube alone was filled with water because the distance from the surface electrodes to the water front in the tube was longer.

From T-π transformation,[15] the T network that is composed of Z_2 and Z_3 in Fig. 3b can be transformed into the π-network that is composed of Z_0 and Z_{12} in Fig. 3c. Then, the equivalent impedance Z_{12} becomes:

$$Z_{12} = \frac{2R}{1+\mathrm{j}\omega CR} + \mathrm{j}\frac{\omega C_{Ei} R^2}{(1+\mathrm{j}\omega CR)^2} = \Re(Z_{12}) + \mathrm{j}\Im(Z_{12}). \qquad (7)$$

Equation 7 is complicated, and the sign of the imaginary part of Z_{12} has the possibility to become positive, i.e., the equivalent element works as an inductor when the sign of the imaginary part is positive[16] under some electrical conditions. An inspection of Eq. 7 using the set of electric constants in Table 2 showed the case that a parallel combination of Z_{12} and the subnetwork of Z_p, i.e., Z_T in Eq. 5, formed an apparent parallel-resonance circuit, even though the circuit model used was composed of only resistors and capacitors. Figure 7 shows the example of the impedance plane figure that exhibits the formation of an apparent parallel-resonance circuit under particular conditions. This local network induces the local peak of the impedance in the high-frequency range. The origin is the introduction of the intermediate electrode that forms capacitor C_{Ei} in the circuit. Another interpretation of the effect of the intermediate electrode is that the electrode segregates the electric field lines in the near-surface zone of the specimen and introduces them into the voltage source as shown in Fig. 1. Accordingly, our method evaluates the electric properties resulting from the remaining electric field lines in the deep zone.

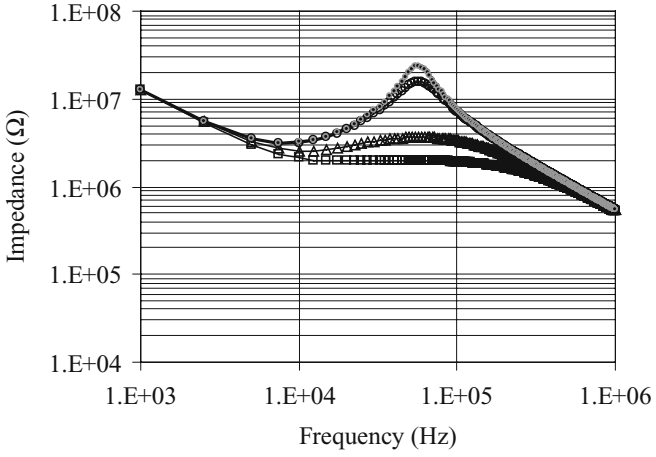

Fig. 8. Effect of the parallel resistance R_p on the impedance. *Squares*, $R_p = 5R$; *triangles*, $R_p = 10R$; *open circles*, $R_p = 100R$; *filled small circles*, $R_p = 1000R$; $R = 500$ kΩ

Table 3. Electric constants for inspecting the effect of the parallel resistance R_p

R_p	R (MΩ)	C (pF)	R_p (MΩ)	C_p (pF)	C_E (pF)	C_{Ei} (pF)
$R_p = 5R$			8			
$R_p = 10R$	0.5	0.8	40	0.3	50	100
$R_p = 100R$			400			
$R_p = 1000R$			4000			

Water distribution, model 3; intermediate electrode width, 40 mm

The existence of parallel resistance R_p was assumed because water is a conductor, and this constant corresponds to that of the core part and may give us useful information about core moisture in a cylindrical body such as a log. The effect of resistance R_p is shown in Fig. 8. The magnitude of R_p affects the intensity and the sharpness of the impedance peak. The sharpness increases with increase of resistance R_p. This simulation result is interesting because the sharpness may indicate the degree of drying in the core part of a log. The change of the magnitude of the impedance becomes small when R_p is larger than $100 \times R$. Table 3 shows the individual constants used in the calculation.

The effect of the intermediate electrode width was also simulated. Taking the spatial arrangement of each electric element into consideration, we can assume (1) increases of the resistances R and R_p and the capacitor C_{Ei} and (2) decreases of the magnitudes of the capacitances C and C_p with increases of the intermediate electrode width. The capacitor C_E, however, does not change. Table 4 shows the individual electric constants obtained from a trial-and-error approach. Figure 9 explains very well the effect of the intermediate electrode width on the impedance frequency responses. The effect of resistor R was minor in the high-frequency range because resistor R forms a parallel connection with capacitor C. The agreement between the simulation

Table 4. Electric constants for inspecting the effect of the intermediate electrode width

Intermediate electrode width	R (MΩ)	C (pF)	R_p (MΩ)	C_p (pF)	C_E (pF)	C_{Ei} (pF)
Narrow (20 mm)	0.25	1.6	1	2.00		50
Middle (40 mm)	0.50	0.8	4	0.30	50	100
Wide (80 mm)	0.70	0.4	80	0.06		200

Water distribution, model 3

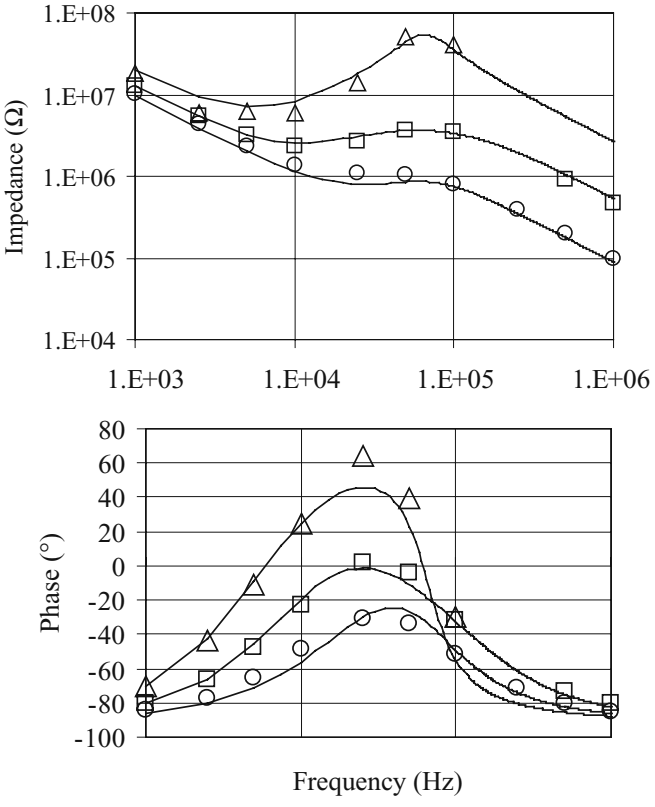

Fig. 9. Effect of the intermediate electrode width on the impedance and the phase. *Symbols*, experiment; *lines*, calculation; *triangles*, wide electrode (80 mm); *squares*, middle-width electrode (40 mm); *circles*, narrow electrode (20 mm)

and the experimental values was also good for the phase diagram, as shown in Fig. 9.

The electric constants obtained here would not be equal to the real values of the body. The real body consists of continuous material. Although further modeling based on the concept of a distributed constant network may give better fittings, the simple discrete model used has explained well the essence of the frequency characteristics of the impedance. The characteristic effects of the intermediate electrode are: (1) that the electrode forms part of a local T-network element in the equivalent network model and induces local parallel resonance, (2) and that the effect reflects the moisture gradient in the cylindrical body. The proposed new impedance measurement system should contribute to nondestructive evaluation of cross-sectional moisture distributions in logs and standing trees.

Conclusions

The proposed impedance measurement system introducing an intermediate electrode enabled the segregation of measurement of the target area in the cylindrical body. The width of the intermediate electrode can regulate the target area. The proposed equivalent electrical network model could represent well the frequency responses of the impedance under different moisture distributions.

References

1. Kogure J, Kawamura H, Onoue M, Yamada H, Tsao JW (1984) Development of a portable X-ray computed tomographic scanner for measuring the annual rings of a live tree. Rigaku Denki J 15:8–15
2. Rosenkilde A, Glover P (2002) High-resolution measurement of the surface layer moisture content during drying of wood using a novel magnetic resonance imaging technique. Holzforschung 56:312–317
3. Nakanishi TM, Okano T, Karakama I, Ishihara T, Matsubayashi M (1998) Three-dimensional imaging of moisture in wood disk by neutron beam during drying process. Holzforschung 52:673–676
4. Kamatani A, Nakao T, Kodama Y (2000) Non-destructive measurement of heartwood moisture content in sugi (*Cryptomeria japonica* D. Don) standing trees by lateral vibration method. Mokuzai Gakkaishi 46:13–19
5. Japan Housing and Wood Technology Center (2000) Approbation of the moisture meters for softwood lumber. http://www.howtec.or.jp/ninsyou/gansuiritsu.html
6. Forrer JB (1984) An electronic system for monitoring gradients of drying wood. Forest Prod J 34(7/8):34–38
7. Sakai M, Hashimoto A (1998) Continuous measurement of moisture distribution in lumber. In: Proceedings of the annual meeting of the Chubu branch of the Japan Wood Research Society (in Japanese). Toyama, August 27, 1998, pp 40–41
8. Sobue N, Inagaki M (2007) Estimation of cross-sectional moisture content in commercial timbers by impedance measurement in RF range. In: Proceedings of the 7th international conference on electromagnetic wave interaction with water and moist substances. Hamamatsu, April 16, pp 123–128
9. Titta M, Savolainen T, Lappalainen T (2003) Electrical impedance spectroscopy applications for wood moisture gradient measurement. In: Proceedings of 5th international conference on electromagnetic wave interaction with water and moist substances. Rotorua, New Zealand, March 24, pp 277–283
10. Sobue N (2000) Measurement of moisture gradient in wood by electrode scanning moisture analysis, ESMA. In: Proceedings of the 12th international symposium on nondestructive testing of wood. Sopron, Hungary, September 14, pp 301–306
11. Suzuki Y (2007) Development of estimating method of moisture content of water distribution of Sugi (Japanese cedar) log using impedance measurements. In: Proceedings of the 7th international conference on electromagnetic wave interaction with water and moist substances, Hamamatsu, April 16, pp 107–113
12. Sobue N, Doi K (2009) Estimation of cross-sectional moisture distribution in cylindrical bodies introducing an intermediate electrode in impedance measurement (in Japanese). In: Proceedings of the 59th annual meeting of the Japan Wood Research Society. Matsumoto, March 17, p 30
13. Murase K, Sobue N (2010) Measurement of moisture distribution in branches and logs using impedance method in high frequency range introducing an intermediate electrode (in Japanese). In: Proceedings of the 60th annual meeting of the Japan Wood Research Society. Miyazaki, March 17, p 118
14. Van Valkenburg ME (1974) Network analysis, 3rd edn. Prentice-Hall, Englewood Cliffs, pp 242–278
15. Van Valkenburg ME (1974) Network analysis, 3rd edn. Prentice-Hall, Englewood Cliffs, p 347
16. Van Valkenburg ME (1974) Network analysis, 3rd edn. Prentice-Hall, Englewood Cliffs, pp 372–387